JOURNAL OF MATERIALS SCIENCE **36** (2001) 1077–1085

Functionally graded cathodes for solid oxide fuel cells

N. T. HART
Dept. of Materials Engineering, Brunel University, Uxbridge, UB8 3PH, UK; Rolls-Royce Strategic Research Centre, PO Box 31, Derby, DE24 8BJ, UK

N. P. BRANDON*
T.H.Huxley School of Environment, Earth Sciences and Engineering, Imperial College of Science Technology and Medicine, London, SW7 2BP, UK
E-mail: n.brandon@ic.ac.uk

M. J. DAY
Rolls-Royce Strategic Research Centre, PO Box 31, Derby, DE24 8BJ, UK

J. E. SHEMILT‡
Dept. of Materials Engineering, Brunel University, Uxbridge, UB8 3PH, UK

Functionally graded Solid Oxide Fuel Cell cathodes have been prepared from mixtures of strontium doped lanthanum manganite (LSM) and yttria stabilised zirconia (YSZ) using screen printing techniques. Samples were characterised using scanning electron microscopy, elemental dot mapping, and electrochemical impedance spectroscopy. Characterisation using AC impedance techniques showed that each cathode could be analysed in terms of a low frequency, mid frequency and high frequency response. Results showed that as the level of YSZ-LSM grading within the cathode increased, the polarisation resistance decreased. No region of the graded cathode should contain less than 20 wt% LSM to prevent an accompanying increase in series resistance.

1. Introduction

Functionally graded materials (FGMs) have been developed as a method of joining dissimilar materials that are usually incompatible [1]. Instead of an abrupt change in composition and/or microstructure between the two materials, FGMs have a graded interface at which the composition gradually changes from one material to the other. As the composition changes, so do the effective material properties, thereby avoiding sharp discontinuities in, for example, thermal expansion coefficients, which could result in delamination during thermal cycling. The objective of this work was to apply this concept to the cathode of a Solid Oxide Fuel Cell (SOFC).

High temperature (700 °C–1000 °C) SOFCs commonly employ an yttria-stabilised zirconia (YSZ) electrolyte, a strontium-doped lanthanum manganite (LSM) cathode and a nickel-YSZ cermet anode [2]. Strontium doped lanthanum cobaltite (LSCO) has been identified as a cathode material that offers improved electrical conductivity, 1200 S cm^{-1} [2] at a temperature of 1000°C compared to a typical value of 150 S cm^{-1} for LSM at the same temperature [2]. Unfortunately LSCO has a higher thermal expansion coefficient (TEC) than the electrolyte (22 to 24 $\times 10^{-6}$ K^{-1} compared to 10.8×10^{-6} K^{-1}) [2]. It has also been shown that LSCO readily reacts with YSZ to form a resistive phase [2].

The use of a mixed LSM/YSZ layer at the cathode–electrolyte interface to improve electrochemical performance is well known. Such electrodes are referred to as composite cathodes and were first reported by Kenjo and Nishiya [3]. It was shown that by adding 50 wt.% YSZ to the LSM cathode, the polarisation resistance could be reduced to 25% of its original value. Subsequent studies showed improvements using a variety of cathode arrangements and fabrication methods [4–11]. The oxygen reduction reaction at the cathode-electrolyte interface requires the co-incidence of gaseous oxygen, an electronic conductor and an ionic conductor, a region known as the triple phase boundary. When a composite cathode is employed, it is widely accepted that the addition of YSZ increases the effective length of the triple phase boundary, improving the electrochemical performance.

Previous work has reported improvements in grading techniques [12–15]. This study sought to compare the behaviour of a family of graded cathodes, each fabricated in a similar manner using the same quantity of

* Author to whom all correspondence should be addressed.
‡ *Present Address*: J. M. & J. E. Shemilt Consultants, 34 Manor Road, Ruislip, Middlesex, HA4 7LB, UK.

LSM and YSZ, but with those materials distributed differently within each cathode. The aim was to try to identify the impact of the different levels of grading on the performance of the cathode.

2. Experimental procedure

The investigation was based on a bi-layer cathode. This consisted of a layer of LSM deposited on the YSZ electrolyte, and a further current collecting layer of LSCO on top of the LSM (Fig. 1), following previous work by Sasaki and Gaukler [13, 14]. A control sample with no grading was prepared along with three further samples with a graded YSZ/LSM microstructure. The grading was carried out over 4 screen printed layers. The number of steps over which the composition changed was altered for each of the samples. Each graded interface was designed to contain the same weight % of YSZ, LSM and LSCO, although the distribution of the YSZ and LSM varied for each sample.

The LSM powder, $La_{0.85}Sr_{0.15}MnO_3$, was supplied by Haldo Topsøe, Denmark with a submicron particle size. This was calcined at 1200°C for 1 hour before being ground by hand using a pestle and mortar, and ball milled in acetone using YSZ milling media for 4 hours. This resulted in a powder with a D_{50} particle size of 3.95 μm. The precursor ink was prepared using a terpineol based binder with a solids loading of 60 wt %. An ultrasonic probe was used to mix the powder with the binder and break down any residual large particles. The LSCO starting powder, $La_{0.8}Sr_{0.2}CoO_3$, (RISØ National Research Laboratory, Denmark) had a submicron particle size and the ink was prepared in a similar way to that described for LSM. To accommodate the larger thermal expansion coefficient of the LSCO, this powder was only milled for 2 hours, resulting in a D_{50} particle size of 5.80 μm. The fired LSCO had a coarse microstructure with a low level of sintering to help it adhere during thermal cycling. The YSZ powder had a particle size of 3–5 μm, and was used as supplied. The appropriate mass of each powder was mixed before the binder was added.

All the samples were fabricated using dense YSZ substrates (TZ8Y, Tosoh, Japan), of 200 μm thickness. The cathode layers were applied to both sides of the substrate, producing a symmetrical half-cell configuration. The cathode structures were built up from 10 screen printed layers. The graded cathodes contained 4 layers of YSZ-LSM, one layer of 100% LSM and 5 Layers of LSCO. A 325 μm mesh screen with a zero thickness emulsion layer was used. Each layer was dried at 100 °C for 30 minutes and allowed to cool before the subsequent print was applied. All the layers were then co sintered at 1125 °C for 1 hour. A ramp rate of 3 °C min^{-1} was used up to 500 °C to allow the binder to burn out, and 5 °C min^{-1} thereafter.

Figure 1 Schematic illustration of the bi-layer cathode used in this study.

TABLE I Details of the samples investigated

Sample	Composition	Total Cathode LayerThickness
1	5 Prints of LSM–5 Prints of LSCO	200 μm
2	4 Prints of 50%LSM/50%YSZ, 1 print of 100% LSM and 5 Prints of LSCO	195 μm
3	2 Prints of 40%LSM/60% YSZ, 2 prints of 40% YSZ/60% LSM, 1 print of 100% LSM and 5 prints of LSCO	200 μm
4	5 Prints of 20%, 40%, 60%, 80%, and 100% LSM (balance YSZ) and 5 prints of LSCO	190 μm

Table I describes the four samples fabricated and investigated in this work. Sample 1 had an ungraded structure, sample 2 was graded over a single step, sample 3 over two steps and sample 4 over four steps. The resultant layers were between 190 μm and 200 μm thick after sintering. Cross sections of the samples were coated with carbon and examined using a JOEL JXA 840A Scanning Electron Microscope with an acceleration voltage of 20 kV. Fracture surfaces were examined to characterise the microstructure and identify any cracks or delamination. Compositional characterisation was carried out on polished cross sections using EDAX dot mapping techniques. The elements zirconium, manganese and cobalt were mapped to identify YSZ, LSM and LSCO respectively. This was carried out over an area of approximately 250 μm × 250 μm. Image analysis techniques were used to interpret the results. The intensity of the traces was measured using commercial image analysis software along with propriety macro programming techniques. These were summed in a direction parallel to the printed layers to generate a one-dimensional histogram. The results represent the density of the elements detected as a function of horizontal position.

Electrochemical Impedance Spectroscopy (EIS) measurements were carried out over a range of temperatures using a Schumberger 1260 frequency response analyser. The sample was supported in a two–electrode arrangement in an alumina holder based on that described in [16]. The test sample was held using springs located outside the heated region. Platinum mesh contacts on the sample surface were connected via platinum wire carried in ceramic sheaths, and a thermocouple was positioned close to the sample to provide an accurate measurement of the sample temperature. The analyser was interfaced to a computer using an IEEE interface card and the results were recorded using commercial software [17]. All the measurements were taken without a DC bias, and spectra were obtained in the 5 mHz to 500 kHz frequency range with an applied voltage amplitude of 20 mV. All the samples were measured in air at temperatures increasing from 700 °C to 1000 °C in 50°C intervals. Further to this, the samples with graded interfaces (i.e. samples 2, 3 and 4) were measured at 700 °C in oxygen-nitrogen mixtures containing 21%, 15%, 10% and 5% oxygen. All data measured on the cathode half cells were corrected for

electrode area, and divided by two to obtain the actual polarisation resistance.

3. Results

3.1. Microstructure

The SEM micrographs of the cross sectional fracture surfaces were similar for all the samples, and a typical example is shown in Fig. 2. The dense YSZ substrate was clearly visible and it was possible to distinguish the LSCO layer from the LSM/YSZ composite region. However it was difficult to distinguish between the different LSM/YSZ layers, indicating that the porosity and structures of the two constituents (YSZ and LSM) were similar. All of the cathodes adhered well to the YSZ substrate and, although there was some evidence of poor contact between the LSM and LSCO, there was no visible cracking between the layers. At a higher magnification it was observed that neck formation had occurred between adjacent particles, and there was evidence that the smaller particles had coalesced to form larger aggregates. Within the composite LSM/YSZ layers large particles of YSZ were observed. These were irregular in shape and as large as 10 μm in some dimensions, larger than the 3–5 μm particle size specified in the supplied powder. The LSCO layer showed the presence of poorly sintered 10 μm to 20 μm agglomerates formed from particles around 1 μm in size.

3.2. Compositional analysis

Fig. 2 shows the region of sample 4, the most graded sample, which was used for elemental dot mapping. The dot mapping results are shown in Fig. 3, and indicate that the intended graded structure was achieved. The zirconium signal was high over the dense YSZ substrate, on the left side of the image, and then gradually declined across the YSZ/LSM interface. The manganese signal increased correspondingly, and the signal for cobalt was constant over the LSCO current collector region. An uneven contoured interface between the LSM and LSCO layer was revealed. This resulted from screen printing onto the underlying LSM layer whilst it was still in the green state, the pressure of the printing screen causing an indentation. The dimensions of the contours were similar in magnitude to the mesh of the screen. Similar print patterns were found in all four samples.

Fig. 4a–d summarises the dot mapping results. Sample 1 (Fig. 4a) showed a sharp decrease in the intensity of zirconium on moving out of the dense YSZ substrate on the left of the trace, region A. The manganese intensity then increased until $\sim$110 μm from the substrate, region B, representing the LSM layer. The cobalt signal increased on reaching the layer of LSCO, region C. The results from Sample 2 (Fig. 4b) show that the zirconium signal fell to an intermediate intensity in region B, representing the 50%YSZ/50% LSM layer. The regions C and D represent the LSM and LSCO current collecting layers respectively. The results from Sample 3 (Fig. 4c) clearly show the two graded YSZ/LSM layers, regions B and C. Regions D and E represent the LSM and LSCO layers respectively. The four step grading of the YSZ/LSM interface in sample 4 is revealed in Fig. 4d. The proportion of LSM increased through regions B to E. There was some evidence of the step changes of the screen printed layers, each having a nominal thickness of approximately 20 μm.

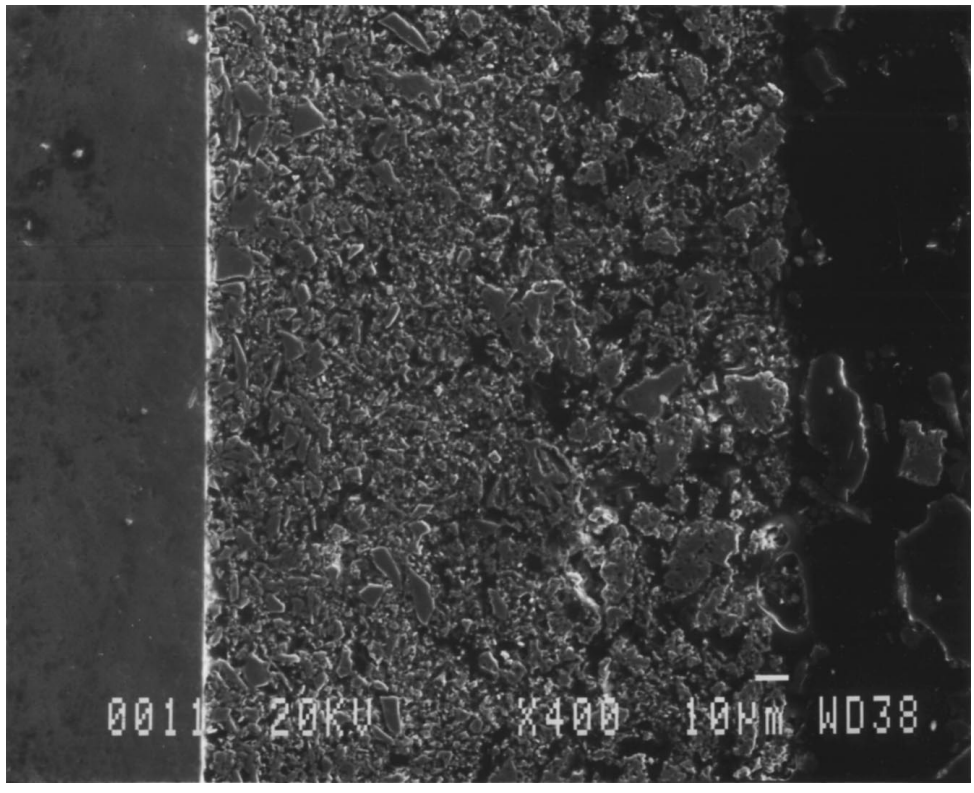

Figure 2 SEM micrograph of a polished cross section of Sample 4, showing the area used for elemental dot mapping.

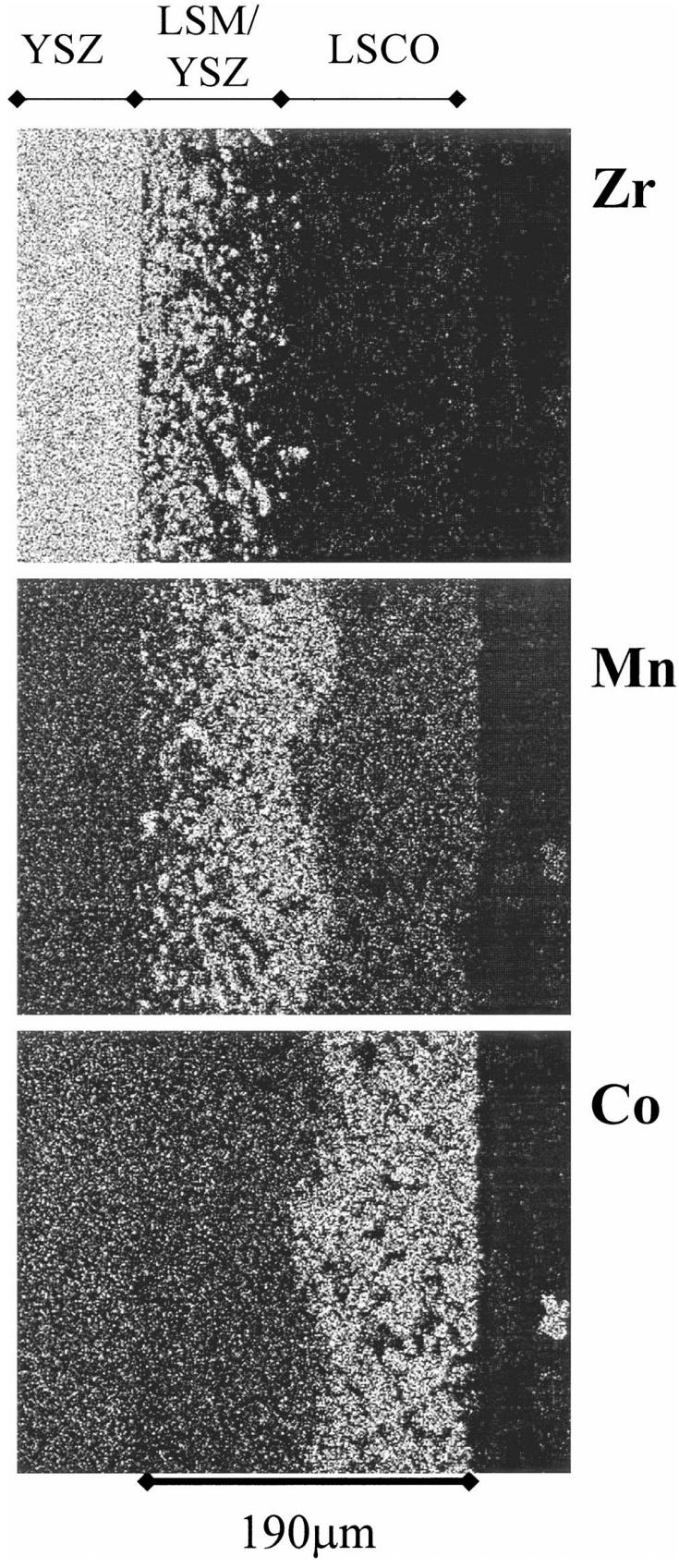

Figure 3 Elemental dot mapping results for Sample 4, showing the elements Zr, Mn and Co.

In all the samples there was a gradual transition between the manganese and cobalt response. This was due in part to the contoured printing pattern at the LSM/LSCO interface. A reduced level of zirconium was observed close to the dense YSZ substrate. This was attributed to particle 'pull out' when polishing the samples.

3.3. Electrochemical impedance spectroscopy

The EIS trace of the ungraded structure (sample 1) produced an arc that was semicircular in shape (Fig. 5) with its maximum at a frequency of approximately 100 Hz. The polarisation resistance was an order of magnitude larger than that seen with the graded samples, 50 Ω cm^2

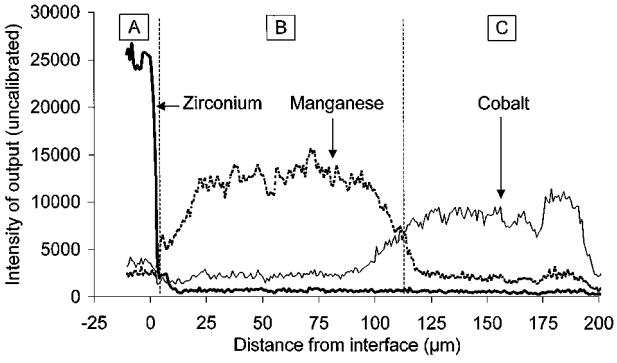

(a)

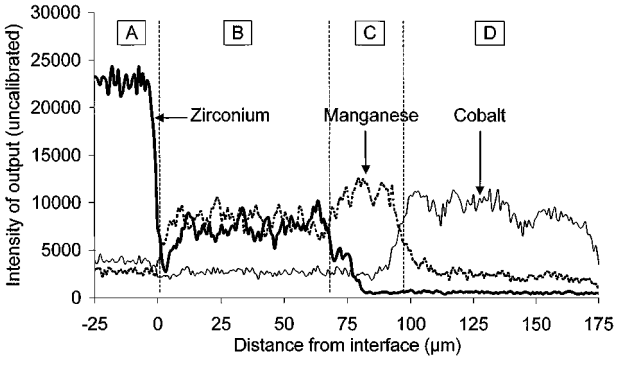

(b)

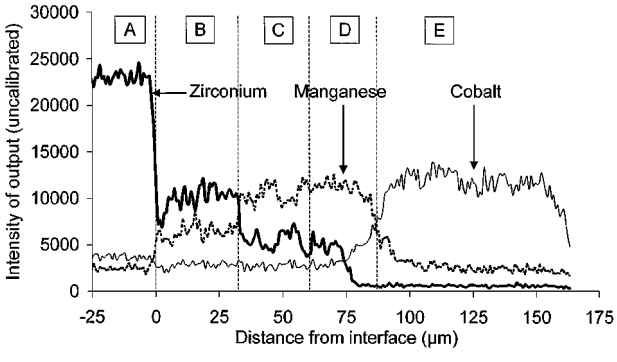

(c)

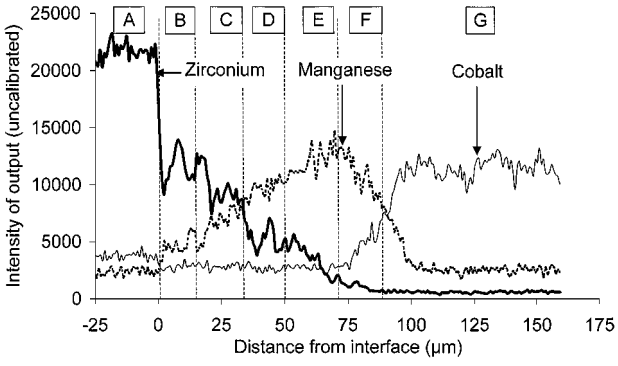

(d)

Figure 4 Elemental dot mapping analysis for (a) Sample 1, (b) Sample 2, (c) Sample 3 and (d) Sample 4, showing the variation in composition with distance from the YSZ interface.

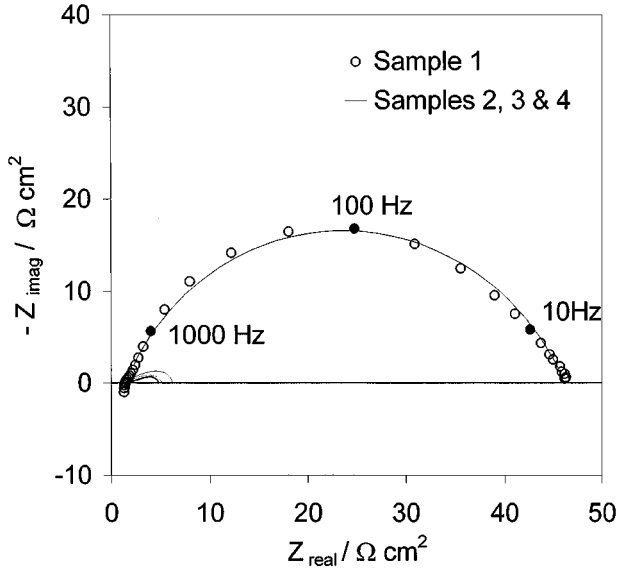

Figure 5 AC impedance spectra of Sample 1 at 700°C in air, compared to the response from Samples 2, 3 and 4 under the same conditions.

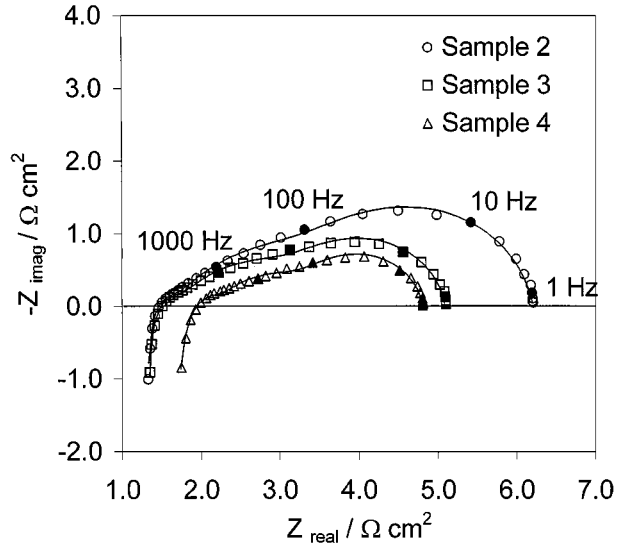

Figure 6 AC impedance spectra of Samples 2, 3 and 4 at 700°C in air.

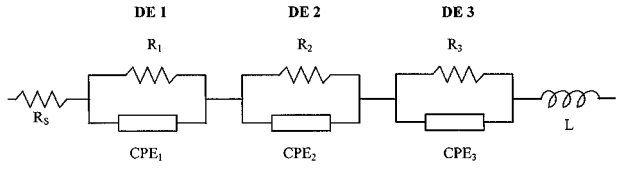

Figure 7 Equivalent circuit used to analyse AC impedance data from Samples 2, 3 and 4.

at 700 °C compared to ≈5 Ω cm^2 for all the graded samples. This improvement was observed across the temperature range.

The samples with graded interfaces produced arcs that were depressed in shape (Fig. 6), with their maximum at a frequency of approximately15 Hz. The curves were fitted to an equivalent circuit using a commercial least squares-fit computer program [18]. The circuit consisted of a series resistance, 3 Distributed Elements and an inductance, all in series (Fig. 7) following previous studies [6, 9, 19]. The distributed elements represent a constant phase element (CPE) in parallel with a resistor which produces a complex plane impedance curve in the form of an arc with the centre displaced from the real axis. Each element has an associated exponent value, Phi, which reflects this displacement. Values of Phi for CPE1, CPE2 and CPE 3 were fixed at 0.93, 0.7 and 0.45 respectively

for all samples. CPE 1 corresponded to the low frequency part of the arc, CPE 2 corresponded to the mid-frequency part of the arc, and CPE 3 the high frequency, and therefore these fitted terms will be referred to as low, mid and high frequency elements (R_{low}, R_{mid} and R_{high}). The series resistance (R_s) represents the sum of the resistance of the electrolyte, the current collectors and the connecting wires, and was evaluated in the least-squares fit procedure. The inductive component arose from the high frequency response of the measuring apparatus, and was fixed at 0.7×10^{-7} H.

The overall polarisation resistance ($R_p = R_{low} + R_{mid} + R_{high}$) showed a similar response to temperature for all the samples and decreased as the temperature increased. The polarisation resistance of sample 2, with a single graded layer, decreased from 5.03 $\Omega\,cm^2$ at 700 °C to 0.92 Ω cm ^{2} at 850°C, and to 0.15 Ω cm^2 at 1000 °C. These values compare well with published values of 12 Ω cm^2 at 700 °C, 0.6 cm ^{2} at 850 °C and 0.12 Ω cm^2 at 1000 °C [5]. When the level of grading was increased to 2 steps (sample 3), the resistance decreased further; 4.09 $\Omega\,cm^2$ at 700 °C, 0.75 $\Omega\,cm^2$ at 850 °C and 0.13 $\Omega\,cm^2$ at 1000 °C. This trend continued as the level of grading increased, with measured values of 3.48 $\Omega\,cm^2$ at 700 °C, 0.68 Ω cm^2 at 850 °C, and 0.11 Ω cm^2 at 1000 °C, when the layer was graded over 4 steps.

Fig. 8 demonstrates that there was a change in activation energy for all three graded samples at a temperature of 850 °C. Below this temperature the activation energy was ∼1.05 eV and above it rose to ∼1.45 eV. Fitted values of the activation energies for all samples are given in Table II.

The series resistance for sample 4 was significantly higher than that of samples 1 and 2 (Fig. 9). For example, at 700 °C, the series resistance of sample 4 was 1.34 $\Omega\,cm^2$, compared to1.20 $\Omega\,cm^2$ for samples 2 and 3. This increase in series resistance will affect the performance of a working fuel cell, and therefore the sum of R_p and R_s was plotted (Fig. 10) to provide an indication of their contribution to the effective area specific resistance of a complete cell. On this basis, it can be seen that the performance of samples 3 and 4 was very similar, and the advantage that sample 4 previously showed over sample 3 was offset by the increase in series resistance.

The low frequency contribution to the polarisation resistance showed the clearest change in activation energy with temperature, as shown in Fig. 11a. At temperatures below 850 °C the activation energy was ∼1.1 eV, and above this temperature ∼1.85 eV. Table III presents activation energies determined from experimental data for all three graded samples at each of the frequency ranges. In general, across the temperature range, the smallest low frequency component of the polarisation

TABLE II Activation energies for the overall polarisation resistance of the graded cathodes

Sample	Activation Energy Low Temp (700°C–850°C)	Activation Energy High Temp (850°C–1000°C)
2	1.05 eV	1.47 eV
3	1.05 eV	1.42 eV
4	1.01 eV	1.51 eV

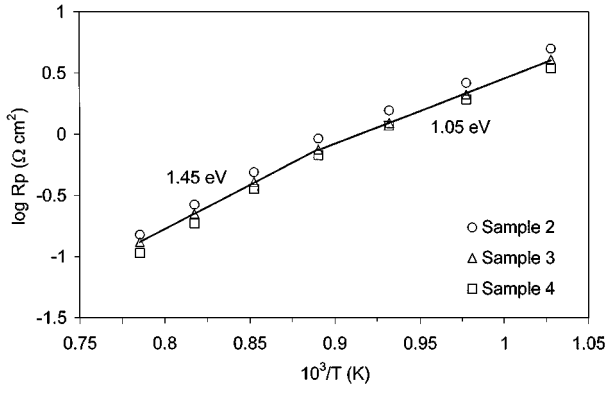

Figure 8 Arrhenius plot of the overall polarisation resistance of Samples 2, 3 and 4 in air.

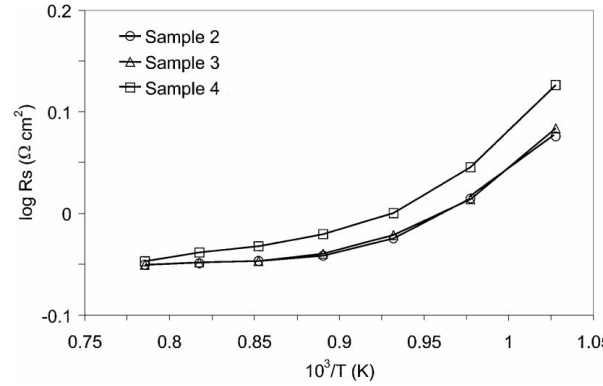

Figure 9 Arrhenius plot of the series resistance of Samples 2, 3 and 4 in air.

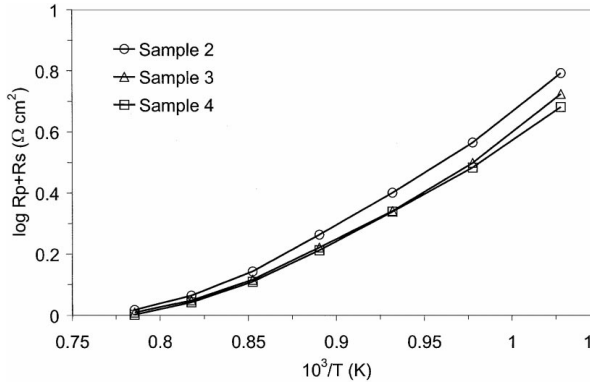

Figure 10 Arrhenius plot of the sum of the polarisation and series resistance for Samples 2, 3 and 4 in air.

TABLE III Activation energies for the low, mid and high frequency contributions to the polarisation resistance of the graded cathodes

	Sample 2		Sample 3		Sample 4	
	Low Temp	High Temp	Low Temp	High Temp	Low Temp	High Temp
Low Freq	1.94 eV	1.16 eV	1.87 eV	1.18 eV	1.79 eV	0.95 eV
Mid Freq	0.88 eV		0.88 eV		0.85 eV	
High Freq	1.40 eV		1.30 eV		1.36 eV	

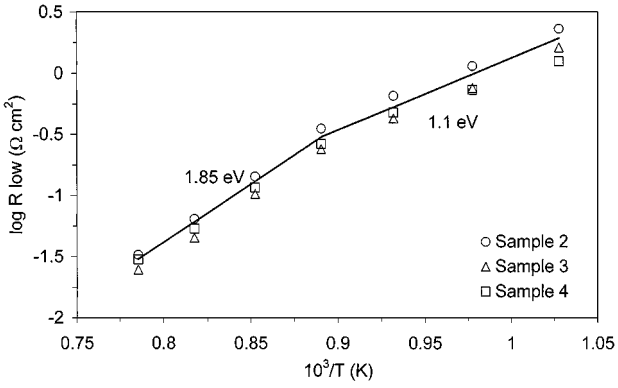

(a)

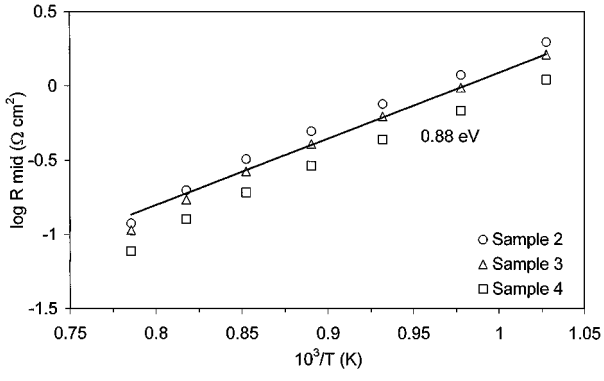

(b)

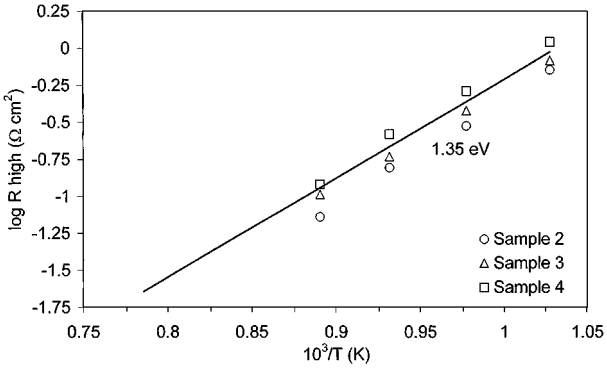

(c)

Figure 11 Arrhenius plot of the (a) low frequency, (b) mid frequency and (c) high frequency contributions to the polarisation resistance of Samples 2, 3 and 4 in air.

resistance was given by sample 3. The Arrhenius plot of the mid frequency element showed a more constant gradient throughout the temperature range (Fig. 11b), with an activation energy ~0.88 eV. Sample 4 gave the lowest resistance for this component. At temperatures above 850 °C only the low and mid frequency arcs were needed to fit the experimental data, so no high frequency element is shown in this temperature region. At lower temperatures the activation energy was around 1.35 eV. Fig. 11c demonstrates that sample 2 gave the lowest resistance for this high frequency component.

When the graded samples were measured in oxygen depleted synthetic air, the EIS response was clearly extended in the low frequency region, while the high frequency region showed little change. This is illustrated in Fig. 12, which describes the results from sample 4 at 700 °C. Fig. 13 illustrates that, on decreasing the oxygen content from 21% to 5%, sample 2 showed

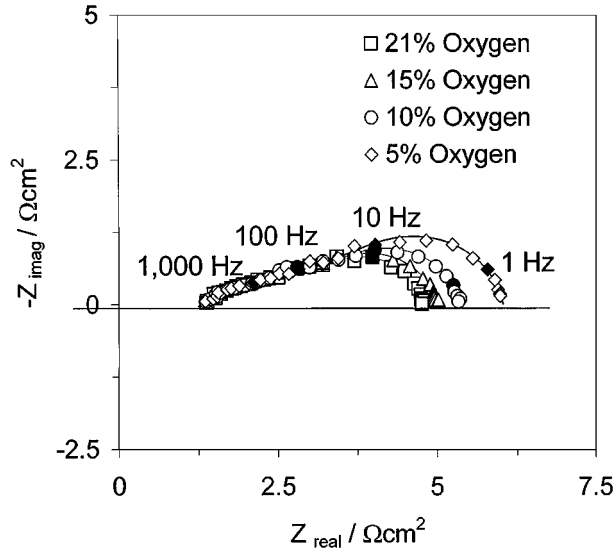

Figure 12 Effect of oxygen depleted synthetic air on the AC impedance response of Sample 4 at 700°C.

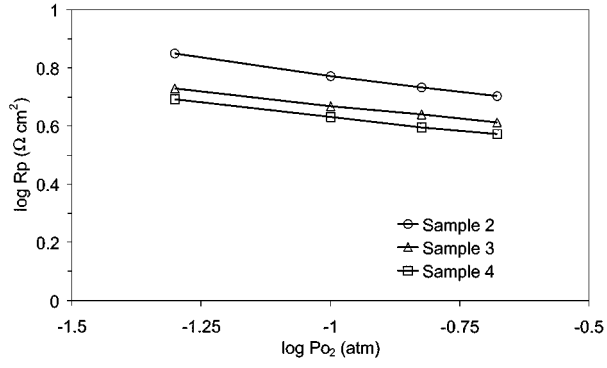

Figure 13 Effect of oxygen partial pressure on the overall polarisation resistance of Samples 2, 3 and 4 at 700°C.

an increase in overall polarisation resistance from 5.06 Ω cm^2 to 7.07 Ω cm^2. The equivalent increase associated with samples 3 and 4 was from 4.10 Ω cm^2 to 5.35 Ω cm^2, and from 3.74 Ω cm^2 to 4.92 Ω cm^2, respectively.

These observations were supported by the results of the curve fitting procedure. The resistance corresponding to the low frequency aspect was sensitive to changes in oxygen partial pressure, while the mid and

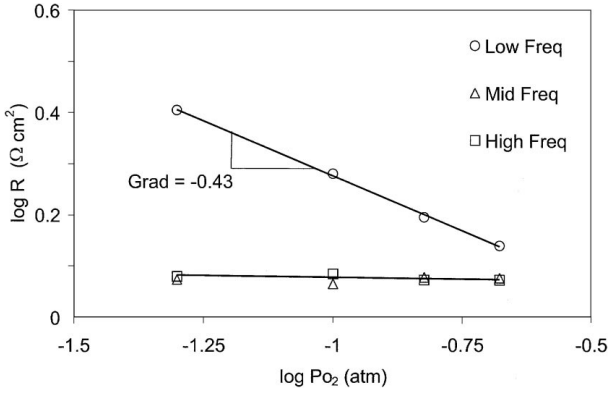

Figure 14 Effect of oxygen partial pressure on the low, mid and high frequency contributions to the polarisation resistance of Sample 4 at 700°C.

high frequency elements were essentially independent. Fig. 14 illustrates the effect of P_{O2} on the low, mid and high frequency contribution to the overall polarisation resistance of sample 4 at 700 °C. The slope of the low frequency element indicates a $P_{O2}^{-0.43}$ dependence.

4. Discussion and conclusion

Van Herle *et al.* [20] proposed that three rate determining processes can occur within the O_2-LSM-YSZ system, each of which can be associated with a different frequency response within the EIS measurement. For the case of non-composite cathodes they proposed oxygen adsorption (high frequency element), oxygen dissociation (mid frequency element) and bulk O^{2-} ion diffusion in the electrode (low frequency element).

Subsequent work by Murray *et al.* on composite cathodes [9], further identified several possible rate determining steps associated with arcs at differing frequencies within their AC impedance data. The authors reported a high frequency response, independent of P_{O2} and with an activation energy around 1.05 eV, which was attributed to YSZ grain boundaries either within the electrode, or at the electrode- electrolyte interface. Also reported was a mid frequency response with an activation energy around 1.49 eV and weak P_{O2} dependence. This was attributed to oxygen dissociation and adsorption rate-limiting steps. A low frequency arc was seen at reduced oxygen partial pressures, which displayed a $P_{O2}^{-0.57}$ dependence, and was tentatively assigned to surface diffusion.

In our work, neither the high frequency nor the mid frequency elements showed significant P_{O2} dependence, with activation energies in air around 1.35 eV and 0.9 eV respectively. The low frequency element displayed a significant change in activation energy at temperatures around 850 °C, and a $P_{O2}^{-0.43}$ dependence at the measurement temperature of 700 °C. This is inconsistent with the P_{O2}^{-1} dependence expected for gas diffusion. The reason for the change in activation energy at a critical temperature in not clear. Similar changes in activation energy have been reported by Manning *et al.* [21] for oxygen surface exchange with YSZ, hence it can be speculated that the behaviour observed in this study reflects a similar process.

Further work is needed before the features seen at low, mid and high frequencies can be assigned to specific rate determining processes within the FGM cathodes. In particular, polarisation studies using a three-electrode arrangement would help elucidate the processes taking place. Nonetheless, it is interesting to note that each of the three graded structures performed best within a different frequency range. Sample 2, the least graded structure, proved best at high frequency; sample 4, the most graded structure, was best at mid frequency; and sample 3, which lay between samples 2 and 4 in terms of grading, gave the best results at low frequency. Further study of the reaction mechanism, related to sample microstructure, may provide a means of improving the performance of both graded and conventional composite cathodes.

As well as considering the response associated with the oxygen reduction processes, the series resistance is also important in determining cell performance. In this study, it has been shown that the series resistance of the most graded sample was higher than that of both other samples tested. This is consistent with previous work [15], in which it was suggested that the increase in series resistance of a graded cathode containing a 20%LSM/80%YSZ layer could be attributed to its poor electronic conductivity, as its composition fell below the percolation limit of LSM. This layer therefore only has the effect of increasing the thickness of the electrolyte. Using literature data for the ionic conductivity of YSZ [22], it can be calculated that, on average across the temperature range, the increase in series resistance for sample 4 in this study corresponds to an increase in effective electrolyte thickness of 15 μm. This prediction compares well with the estimated thickness of 20 μm for each sprayed layer, confirming that a 20%LSM/80%YSZ layer should be avoided.

Acknowledgements

N. Hart is supported by an Engineering and Physical Sciences Research Council (EPSRC) Eng-D Studentship and sponsored by Rolls-Royce plc.

References

1. M. KOIZUMI, "The Concept of FGM, Functionally Gradient Materials, Ceramic Trans, Vol. 34" (Am. Ceram. Soc., 1993) p. 3.
2. N. Q. MINH and T. TAKAHASHI, "Science and Technology of Ceramic Fuel Cells" (Elsevier Science, Amsterdam, 1995).
3. T. KENJO and M. NISHIYA, *Solid State Ionics* **57** (1992) 295.
4. M. J. L. OSTERGARD, C. CLAUSEN, C. BAGGER and M. MOGENSEN, *Electrochim. Acta* **40** (1995) 1971.
5. M. JUHL, S. PRIMDAHL, C. MANON and M. MOGENSEN, *J. Power Sources* **61** (1996) 173.
6. M. J. JORGENSEN, S. PRIMDAHL and M. MOGENSEN, *Electrochemica Acta* **44** (1999) 4195.
7. P. HOLTAPPELS, M. J. JORGENSEN, S. PRIMDAHL, M. MOGENSEN and C. BAGGER, in "Proc. 3rd European SOFC Forum," edited by P. Stevens (Nantes, France, June, 1998) p. 311.
8. M. JUHL, S. PRIMDAHL and M. MOGENSEN, in "Proc. 17th Risoe Int. Symp. on Mat. Sci., Sep.," edited by F. W. Poulsen, N. Bonanos, S. Linderoth, M. Mogensen and B. Zachau-Christiansen (Roskilde, Denmark, 1996) p. 295.
9. E. P. MURRAY, T. TSAI and S. A . BARNETT, *Solid State Ionics* **110** (1998) 235.
10. T. TSAI and S. A. BARNETT, *ibid.* **93** (1997) 207.
11. T. TSAI and S. A. BARNETT, in "Proc. 5th Int. Symp. SOFCs, Electrochem. Proc. Vol. 97-40," edited by U. Stimming, S. C. Singhal, H. Tagawa and W. Lehnert (Aachen, Germany, 1997) p. 368.
12. M. NAGATA, C. IWASAWA, Y. SEINO, H. YAMAMOTO and M. ONO, in Proc. 2nd Int. Fuel Cell Conf. (Kobe, Japan, Nedo, 1996) p. 255.
13. K. OIZUMI and L. GAUCKLER, *Proc. Int. Symp. Stuct. Func. Grad. Matter* **3** (1995) 651.
14. K. SASAKI, M. GODICKEMEIER, P. BOHAC, A. ORLIUKAS and L. J. GAUKLER, in 5th IEA-Workshop SOFCs (Julich, Germany, 1993) p. 187.
15. C. BAGGER, S. LINDEROTH, M. MOGENSEN, P. V. HENDRIKSEN, B. KINDL, S. PRIMDAHL, P. H. LARSEN, F. W. POULSEN, N. BONANOS and M. J. JORGENSEN, in "Proc of 6th Int. Symp. SOFCs, Electrochem. Proc. Vol. 99-19," edited by S. C. Singhal and M. Dokiya (Honolulu, Hawaii, Oct., 1999) p. 28.
16. J. R. MACDONALD (ed.), "Impedance Spectroscopy" (John Wiley & Sons, New York, 1987).
17. Z Plot for Windows Version 2. Scribner Associates Inc. (1997).

18. X-View for Windows Version 1.5b. Scribner Associates Inc. (1996).
19. F. P. F. VAN BERKEL, F. H. VAN HEUVELN and J. P. P. HUIJSMANS, *Solid State Ionics* **72** (1994) 240.
20. J. VAN HERLE, A. J. McEVOY and R. THAMPI, *Electrochimica Acta*. **41**(9) (1996) 1447.
21. P. S. MANNING, J. D. SIRMAN and J. A. KILNER, *Solid State Ionics* **93** (1997) 125.
22. U. G. BOSSEL, "Facts and Figures" (Swiss Federal Office of Energy, Berne, Switzerland, 1992).

Received 3 May
and accepted 7 June 2000